Linear Viscoelastic Predictions of a Consistently Unconstrained Brownian Slip-Link Model

Deepa M. Nair and Jay D. Schieber*

Department of Chemical and Environmental Engineering, Illinois Institute of Technology, Chicago, Illinois

Received August 31, 2005; Revised Manuscript Received March 1, 2006

ABSTRACT: A consistently unconstrained Brownian slip-link (CUBS) model with constant chain friction is used to predict the linear rheological behavior of linear, entangled polymeric liquids. As in the previously proposed slip-link model without constraint release (*J. Rheol.* **2003**, *47*, 213), this model contains segment connectivity, contour-length fluctuations, and chain stretching in a self-consistent and natural way. Constraint release is considered in a mean-field way, but including fluctuations, both as a binary interaction between chains, and as a multichain interaction. Unlike previous mean-field works, constraint release is included on the level of chain dynamics instead of assuming that the relaxation modulation is a product of two moduli found by independent processes. These dynamics require no additional parameters. The model may also be used to make nonlinear flow predictions without any additional parameters. We find that inclusion of the additional physics of constraint release improves the linear viscoelastic predictions of the model, both for monodisperse polymers and bidisperse polymer blends. The difference between binary and multichain interaction predictions is not sufficiently large to distinguish comparisons with data within uncertainty.

1. Introduction

The dominant paradigm for understanding entangled polymer dynamics is the tube model[1−6] with its many incarnations.[7−24] The tube is a simple picture used to mimic the constraints provided by other chains surrounding a test chain. The tube is occupied by an elastic chain that slides back and forth from Brownian forces; when the chain wholly exits a tube segment, that tube segment dies, while another segment is created at the other end of the tube. Hence, during flow, the tube orientation changes by affine motion only, and its lifetime is decided by the chain sloshing around inside. The many tube models in existence vary in the physics included, but also in the level of description used and the mathematical details of the implementation. Cruder levels of description, while easier or faster computationally, typically require the use of uncontrolled mathematical approximation such as pre-averaging.

The original model by Doi and Edwards considered the tube as a static object. However, small-amplitude oscillatory shear flow experiments make clear that chain−chain interactions are important because blends do not exhibit G^* curves that are a simple, linear superposition of monodisperse G^* measurements. Hence, the tube picture required modification, whereby the tube dynamics were now also modified by the relaxation of the surrounding environment, namely by other, diffusing chains. Such a motion is called "constraint release" (CR). Graessley[25] was the first to propose a hopping motion of individual tube segments in order to incorporate this CR process. Orwoll and Stockmayer[26] showed previously that such a hopping motion of Kramer's freely jointed, bead-rod chains yielded relaxation equivalent to a Rouse, free-draining, bead-spring chain.[27] Therefore, Graessley assumed that the relaxation modulus of a chain in a tube undergoing CR would be the product of the reptation process and a Rouse relaxation spectrum. However, in his calculation, only a single hopping frequency is assumed, which is determined by a certain moment of the waiting time for the destruction from the reptation motion.

* Corresponding author. E-mail: schieber@iit.edu.

As pointed out by Rubinstein and Colby,[10] when this procedure is used, along with relaxations including contour-length fluctuations (CLF) of the chain inside the tube, relatively poor agreement is found with data. In fact, the results can be worse than simple linear superposition. The remedy suggested by Rubinstein and Colby was to use a *spectrum* of hopping frequencies, all found from the reptation motion of the (constant-contour-length) chain inside the tube. Still, the resulting relaxation modulus was assumed to be a product of these two relaxation functions: one from constraint release, and one from an elastic chain in a fixed tube.

Likhtman and McLeish[24] further refined this approach by using a more-sophisticated expression for relaxation involving contour-length fluctuations and Rouse-like motions of the chain in the tube. The resulting equations were found to describe well the G^* experiments of polystyrene. These authors also assumed that the relaxation modulus was the product of these two different dynamics: reptation and CLF on one hand, and CR on the other. Similarly, the model makes only linear viscoelastic predictions and is not applicable to flows. In addition, the authors introduced an adjustable parameter c_v, which allows the hopping distance from a CR event to be less than the tube diameter. Agreement with experiment required the authors to set $c_v = 0.1$. The work by Likhtman and McLeish then requires three parameters: a time scale τ_e, an entanglement modulus G_e, and the dimensionless parameter c_v, and is often considered to be state of the art.[28]

In this work, we study the same physical ideas but on a slightly more fundamental level. Namely, we no longer assume that the relaxation modulus is the product of two relaxation processes found by independent means. Instead, constraint release is imposed on the level of the dynamics of the chain, and the relaxation modulus follows from these rigorously. Second, we show how a straightforward calculation can be used to estimate that the parameter c_v be set to 1/12. Third, the model used is not a tube model, but rather a mean-field, single-chain, slip-link model, or temporary network model, with a single

10.1021/ma0519056 CCC: $33.50
Published on Web 04/07/2006

phenomenological time constant, τ_e. To mimic the effects of constraint release, the network junctions, or slip-links, are allowed to diffuse, with a diffusion coefficient determined by the lifetimes of the entanglements as suggested by Rubinstein and Colby. Hence, the model is called consistently unconstrained Brownian slip-links, or CUBS. Finally, aside from allowing us to study state-of-the-art constraint release ideas on a more fundamental level, a possibly greater advantage to our approach, is that the resulting model is also applicable to flows. Therefore, we introduce here a reptation-like model that incorporates contour-length fluctuations, segment connectivity, monomer density fluctuations, entanglement fluctuations, and constraint release, which is applicable to LVE and flows. Moreover, these effects are included naturally in the dynamics of the model, rather than being added by hand with additional adjustable parameters.

In the following section, we explain the mathematical details of the CUBS model, including a description of the parameters, dynamics, and stress-tensor expression. In Section 3, the numerical algorithm used to calculate model predictions is given. Comparisons are made to analytic equilibrium results to verify our code, and Section 4 describes the experimental systems examined. Section 5 gives comparisons with nearly monodisperse systems, followed by a section showing comparisons with binary blends. Section 5 also compares the molecular-weight scaling of the zero-shear-rate viscosity with experiments on systems of narrow molar mass. Predictions for diffusion coefficients are also shown. These comparisons show that constraint release improves somewhat the linear viscoelastic predictions of both monodisperse and bidisperse systems. Most comparisons show only mild sensitivity to the number of chains assumed to make up an entanglement, justifying earlier "double reptation" assumptions.

2. CUBS Model

Unlike our previously studied slip-link model,[29−31] the model used here includes constant chain friction and constraint release. The slip-link model is related to the transient network model first proposed by Yamamoto and later developed by Lodge, Phan-Thien, Tanner, Fuller, Leal, and others.[27,32] The model is inspired by the success of network theory in rubber elasticity proposed by Guth and Mark in 1934 and later developed by Green and Tobolsky.[33] The slip-link picture was first introduced by Doi and Edwards[4] in 1978. However, their picture was used only to motivate a specific equation relating stress to chain conformation, derived from network theory. No dynamics were modeled based on slip-links. Unlike the traditional network models, in CUBS, the number of Kuhn steps in an entangled strand is treated as a dynamic fluctuating quantity rather than a fixed parameter.

To construct the model, we begin with the chain as a random walk of N_K Kuhn steps, each of length a_K (See Figure 1). With probability $1/N_e$, we add an entanglement (or slip-link) to each step. In the limit of large N_e and N_K ($\gg 1$), this leads to an analytic expression for the distribution of Kuhn steps N_i between entanglements, and a Poisson distribution in the number of entanglements on a chain. The connector vector between entanglements $\boldsymbol{Q}_i$ has a Gaussian conditional distribution. We have shown previously[31] that these statistics arise for the free energy expression

$$F(T,\Omega) = \sum_{i=2}^{Z-1} F_S(T,Q_i,N_i) + F_E(T,N_1) + F_E(T,N_Z) \quad (1)$$

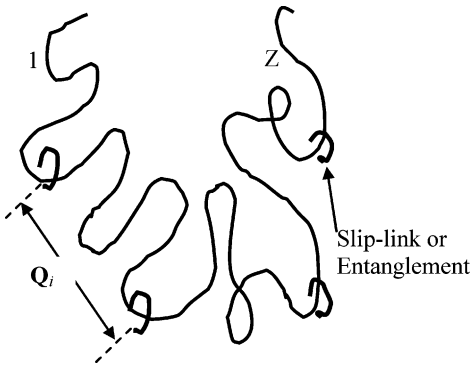

Figure 1. Sketch of the CUBS model.

where F_S is the free energy of the interior, entangled strands, F_E is the free energy of end strands, and the chain conformation is given the shorthand $\Omega = \{\{\mathbf{Q}\}_{i=2}^{Z-1},\{N\}_{i=1}^{Z},Z\}$. The free energies are

$$\frac{F_S(N_i,\mathbf{Q}_i)}{k_BT} = \frac{3\mathbf{Q}_i^2}{2N_i a_K^2} + \frac{3}{2}\log\left(\frac{2\pi a_K^2 N_i}{3}\right) \quad (2)$$

for the entangled strand, and for the dangling ends

$$\frac{F_E(N_i)}{k_BT} = -\frac{1}{2}\log(N_i) \quad (3)$$

Actually, this latter expression is chosen for numerical convenience, and not for physical reasons. It is hoped that the resulting dynamics are not sensitive to this choice. Current work is underway to eliminate this assumption entirely. The equilibrium distribution of the chain conformation is given by the (modified) Maxwell−Boltzmann relation

$$p^{eq}(\Omega) = J^{-1}\exp\left[-\frac{F(\Omega)}{k_BT}\right]\delta(N_K - \sum_{i=1}^{Z} N_i)\exp\left(\frac{\upsilon Z}{k_BT}\right) \quad (4)$$

where J is a normalization constant, F is the free energy of the chain, k_B is the Boltzmann constant, T is temperature, and υ is the chemical potential conjugate to Z. The expression is modified by a Dirac delta function, which ensures that the total number of Kuhn steps in the chain is constant, and a grand-canonical exponential term for Z. It has been shown that setting $\upsilon = \log N_e$ gives the correct statistics.[30]

Substituting the free energy expression in the Maxwell−Boltzmann relation yields:

$$p^{eq}(\Omega) = \frac{\sqrt{N_1 N_Z}}{J\beta^Z}\delta(N_K - \sum_{i=1}^{Z} N_i)\prod_{i=2}^{Z-1}\left(\frac{3}{2\pi N_i a_K^2}\right)^{3/2} \exp\left(-\frac{3\mathbf{Q}_i^2}{2N_i a_K^2}\right) \quad (5)$$

where,

$$\beta = \exp\left(-\frac{\upsilon}{k_BT}\right) \quad (6)$$

When N_e is assumed to be sufficiently large to allow considering N_i as continuous, the normalization constant J is obtained by integrating eq 5 over all possible values of $\{\boldsymbol{Q}_i\}$ and $\{N_i\}$ and then summing over all possible values for Z.

$$J = \frac{1}{\beta}\exp\left(\frac{N_K}{\beta}\right) \tag{7}$$

From eqs 5 and 7, the equilibrium distributions for Z, N, and $\boldsymbol{Q}$ can be obtained.[30,31]

$$P^{eq}(Z) = \frac{1}{J\beta^Z}\frac{N_K^{Z-1}}{(Z-1)!} \tag{8}$$

$$p^{eq}(N) = {N_e}^{-1}\exp\left(-\frac{N}{N_e}\right) + \exp\left(\frac{-N_K}{N_e}\right)\delta(N_K - N) \tag{9}$$

$$p^{eq}(\mathbf{Q}) = \frac{3}{2\pi\mathbf{Q}{N_e}{a_K}^2}\exp\left(-\sqrt{\frac{6\mathbf{Q}^2}{N_e{a_K}^2}}\right) \tag{10}$$

These analytical expressions are used for verifying our numerical algorithm. For situations where the number of Kuhn steps may not be taken as continuous, analytic results are also available.[31]

The dynamic variables used in the model are: the number of entanglements (slip-links) in the chain ($Z(t) - 1$), the number of Kuhn steps in a strand, $N_i(t)$, where $i = 1, ..., Z$, and the position vector of each entanglement, $\boldsymbol{R}_i(t)$, where $i = 1, ..., Z - 1$. There are $Z(t)$ strands in the chain and, hence, $Z - 1$ entanglements and $Z - 2$ entangled strands. The total number of strands, $Z(t)$, fluctuates because of the creation and destruction of entanglements, and the average number of strands at equilibrium is calculated as $\langle Z\rangle_{eq} = M_w/M_e$, where M_w is the weight-average molecular weight and M_e is the entanglement molecular weight. The length of an entangled strand, $\boldsymbol{Q}_i(t) = \boldsymbol{R}_i - \boldsymbol{R}_{i-1}$, is the vector connecting two entanglements, where $i = 2, ..., Z - 1$.

The value of $\boldsymbol{Q}_i$ changes by means of three processes: creation and destruction of entanglements at the ends, diffusion of the surrounding chains (constraint release), and externally imposed flow, which is assumed to be affine. Because of chemical potential imbalances and Brownian forces, Kuhn steps are shuffled across the entanglements. Hence, the number of Kuhn steps in a strand, $N_i(t)$, is a fluctuating quantity, whereas the total number of Kuhn steps in the chain (N_K) is a constant.

The ends of the chain are not constrained by any slip-links and are free to explore all conformations in space. Hence, they have no specified orientation vector. An entanglement is assumed to be destroyed when an end strand completely slips out of a slip-link and the dangling end has zero Kuhn steps. A new entanglement is created when a surrounding chain entangles the test chain at the end, and these creation and destruction processes are related by detailed balance. Detailed mathematics is given below.

Previously, the entanglements were assumed to move affinely. Hence, at equilibrium, the slip-links were fixed in space, until they were destroyed by chain abandonment. In other words, the entanglements were created and destroyed only at the ends of the chain, and there was no constraint release. In this model, we consider the diffusion of the surrounding chains, thereby mimicking the creation and destruction of entanglements in the middle of the chain (constraint release). Also, in the previous model, friction was assumed to be proportional to the number of entanglements, and hence, total friction in the chain fluctuated with the creation and destruction of entanglements. In the present model, friction is assumed to be proportional to the number of monomers or Kuhn steps in the chain. Hence, total friction in the chain is constant because the total number of monomers or Kuhn steps in the chain is constant. Even though we will show that constant chain friction does not affect the $G^*(\omega)$ predictions substantially, it appears to be important in nonlinear flows, which will be discussed in more detail in a subsequent paper.

The evolution equation for the chain conformation probability density at equilibrium has three contributions[34]

$$\frac{\partial p}{\partial t} = \dot{p}_{steps} + \dot{p}_{CR} + \dot{p}_{ends} \tag{11}$$

The right side represents, respectively, the shuffling of Kuhn steps across entanglements, constraint release, and the creation−destruction dynamics at the dangling ends.

Because of imbalance in chemical potential and Brownian forces, Kuhn steps are driven across the entanglements. These processes are assumed to be jump processes, instantaneous on the time scales resolved by the model. In the continuous-N limit, these jump processes are described by the Fokker−Planck equation

$$\dot{p}_{steps} = \sum_{i,j=1}^{Z}\frac{\partial}{\partial N_i}\frac{1}{k_BT}\hat{A}_{ij}\left[\left(\frac{\partial F}{\partial N_j}\right)_{T,\{R_j\}} p + k_BT\frac{\partial p}{\partial N_j}\right] \tag{12}$$

We have considered two possible implementations for the monomeric friction coefficient implicit in the matrix $\hat{A}_{ij}$: constant entanglement friction and constant chain friction. For constant entanglement friction, we set the time scale associated with the motion of Kuhn steps across the entanglement, $\tau_K \sim$ constant, and $\hat{A}_{ij}$ is the Rouse matrix.[27] For constant chain friction, $\hat{A}_{ij}$ is defined as:

$$\hat{A}_{ij} = \begin{cases} -\dfrac{1}{\tau_{i-1}} & i = j+1 \\ \dfrac{1}{\tau_i} + \dfrac{1}{\tau_{i-1}} & i = j \\ -\dfrac{1}{\tau_i} & i = j-1 \\ 0 & \text{otherwise} \end{cases} \tag{13}$$

where

$$\tau_i = \frac{\tau_K}{2N_e}(N_i + N_{i+1}), \qquad i = 1, ..., Z-1 \tag{14}$$

Equations 13 and 14 are modifications of the previously proposed model,[30] taking account of the fact that chain friction is now proportional to the total number of Kuhn steps in the chain. Here, end effects make the chain friction not strictly constant. Hence, fluctuations from end effects are neglected purely for mathematical convenience (an Itô-interpreted SDE introduces no spurious drift terms). The stochastic differential equation equivalent to the above Fokker−Planck equation for Kuhn step shuffling is

$$dN_i = -\sum_j \hat{A}_{ij}\left(\frac{\mu_j}{k_BT}\right)dt + \sqrt{2}\sum_j \hat{B}_{ij}\,dW_j \tag{15}$$

where W_j is the stochastic noise term on entanglement j (called a Wiener process), which describes the random fluctuations imposed by the Brownian forces. μ_j is the chemical potential on strand j, which is obtained from the free energy of the chain

$$\mu_j = \left(\frac{\partial F}{\partial N_j}\right)_{T,\{R_j\},\{N_{i\neq j}\}} \tag{16}$$

and $\hat{B}_{ij}$ is a matrix defined as

$$\hat{B}_{ij} = \frac{1}{\sqrt{\tau_j}}(\delta_{ij} - \delta_{i-1,j}) \tag{17}$$

where δ_{ij} is the Kronecker delta.

Entanglements are created and destroyed at the ends of the chain. The creation and destruction rates are related through detailed balance.[35] The transition probability for creation and destruction processes is given by a master equation

$$\dot{p}_{\text{ends}} = \int [W(\Omega|\Omega')p(\Omega') - W(\Omega'|\Omega)p(\Omega)]\, \mathrm{d}\Omega' \tag{18}$$

where $W(\Omega'|\Omega)$ is the transition probabilities per unit time that a chain with a configuration Ω jumps to configuration Ω'. From detailed balance, we have

$$W^{\text{d}}(\Omega|\Omega')p^{\text{eq}}(\Omega') = W^{\text{c}}(\Omega'|\Omega)p^{\text{eq}}(\Omega) \tag{19}$$

where $W^{\text{c}}(\Omega'|\Omega)$ and $W^{\text{d}}(\Omega|\Omega')$ are the transition probabilities for the creation and destruction of entanglements, respectively. The probability for the destruction of an entanglement at a dangling end W_{d} is proposed as

$$W_{\text{d}}(N_{\text{E}}) = \frac{1}{\tau_{\text{e}}}\sqrt{\frac{3N_{\text{e}}}{N_{\text{E}}}} \tag{20}$$

where N_{E} is the number of Kuhn steps in a dangling end, and $\tau_{\text{e}} = N_{\text{e}}{}^2\tau_{\text{K}}$. This expression is chosen for mathematical convenience for reasons closely related to our assumption for the free energy of the dangling ends. We are currently examining the effect of this assumption by its removal using a more fundamental model. From eqs 19 and 20 and using the Maxwell−Boltzmann relation, the probability for the creation of an entanglement is[30,36]

$$w_{\text{c}}(N_{\text{E}}) = \frac{1}{\tau_{\text{e}}}\sqrt{\frac{3}{N_{\text{e}}N_{\text{E}}}}(N_{\text{E}} - 2) \tag{21}$$

We also impose a cutoff on the entanglement spacing. We restrict the length of a segment to be greater than the length of a Kuhn step, through a reflecting boundary condition.

Similar to what was assumed by Graessley, Rubinstein, and Colby, and Likhtman and McLeish, constraint release is mimicked by a diffusive process of the entanglements. In our model, CR could instead by modeled by a jump process. However, we choose to make the model conform more closely to previous attempts, to examine the typical assumptions. Hence, we write

$$\dot{p}_{\text{CR}} = \sum_{i,j=1}^{Z-1} \frac{\partial}{\partial \boldsymbol{R}_i}\cdot\frac{N_{\text{e}}{a_{\text{K}}}^2}{12k_{\text{B}}T\tau_j^{\text{CR}}}A_{ij}\left[p\left(\frac{\partial F}{\partial \boldsymbol{R}_j}\right)_{T,\{N_j\},\{R_{\neq j}\}} - k_{\text{B}}T\frac{\partial p}{\partial \boldsymbol{R}_j}\right] \tag{22}$$

where τ_j^{CR} is the constraint release time scale, chosen from the distribution of entanglement lifetimes (described in more detail below). Note that use of this expression is equivalent to setting c_v to 1/12 in the Likhtman and McLeish approach. This value is derived in the Supporting Information. Thus, by considering the diffusion of the surrounding chains, we are mimicking the birth and destruction of slip-links in the middle of the chain. The stochastic differential equation for the position of entanglements equivalent to the above expression is

$$\mathrm{d}\boldsymbol{R}_i = \kappa\cdot\boldsymbol{R}_i\,\mathrm{d}t - \frac{N_{\text{e}}{a_{\text{K}}}^2}{12k_{\text{B}}T\tau_i^{\text{CR}}}\left(\frac{\partial F}{\partial \boldsymbol{R}_i}\right)_{T,\{N_i\},\{R_{i\neq j}\}}\mathrm{d}t + \sqrt{\frac{N_{\text{e}}{a_{\text{K}}}^2}{6\tau_i^{\text{CR}}}}\,\mathrm{d}W_i \tag{23}$$

The values for τ_i^{CR} are obtained in a self-consistent way by keeping track of the fraction of surviving entanglements during a simulation. In our model, we consider that entanglements are interactions between 5.4 chains, based on the Cornet criterion[37,38] (see Section B of the Supporting Information). We have also considered binary interactions for entanglements.

To find the new parameters, we call $f(t)$ the fraction of entanglements that have not been abandoned by the test chain from $t = 0$ to the current time t. Then, assuming chain abandonment from an entanglement is independent of other chains making up that entanglement (the only assumption possible in such a mean-field model), the fraction of surviving entanglements $\psi(t)$ is given by

$$\psi(t) = 1 - [1 - f(t)]^{n_{\text{c}}-1} \tag{24}$$

According to experiment, the Cornet criterion suggests the number of chains making up an entanglement is $n_{\text{c}} = 5.4$.

Note, however, that the rate of entanglement abandonment by the test chain may itself be influenced by CR. In other words, $f(t)$ depends, in general, on whether constraint release is taking place. In previous works, the influence of CR on $f(t)$ was ignored. Here, however, we can find $\psi(t)$ in a self-consistent way, taking into account the influence of CR on $f(t)$. This coupling is found by the following procedure. First, we perform a simulation without constraint release. The fraction of surviving entanglements $f(t)$ is obtained as a function of time. From a fit to $\psi(t)$ using eq 25, the constraint-release relaxation spectrum is obtained. The fit is done by using an implementation of the nonlinear least-squares (NLLS) Marquardt−Levenberg algorithm to the form

$$\psi(t) = \sum_i P_i\left(\frac{t}{\tau_i^{\text{CR}}} + 1\right)\exp\left(-\frac{t}{\tau_i^{\text{CR}}}\right) \tag{25}$$

Here, P_i is a set of weight factors corresponding to the constraint-release time constants τ_i^{CR}. This particular form for each mode is the only form that has a single time constant and the correct initial slope. The set of $\{P_i, \tau_i^{\text{CR}}\}$ values obtained from the fit are used in the code, and a simulation with constraint release is performed. In other words, every entanglement at the time of its creation is assigned a CR time constant τ_i^{CR} with probability P_i. The resulting fraction $f(t)$ is again fit to eq 25, and the set of $\{P_i, \tau_i^{\text{CR}}\}$ values are put back into the code. Simulations are thus repeated until the $\psi(t)$ curve converges. Typically, two iterations of this procedure are sufficient to find f and ψ. An example of such a fit is shown in the Supporting Information.

For stress predictions, the model contains two parameters: the average number of Kuhn steps in an entangled strand, N_{e}, and a characteristic time scale for strand relaxations, τ_{e}, which is fit by linear viscoelastic predictions. N_{e} can be estimated from static measurements by using the Cornet criterion, and its value varies with the type of polymer system used.[37,38] $\tau_{\text{e}} = N_{\text{e}}{}^2\tau_{\text{K}}$, where τ_{K} is the time scale associated with the motion of Kuhn steps across the entanglement.

The polymer contribution to the stress tensor is given by thermodynamics arguments[31,34] to be

$$\tau^p = -n \int \int \sum_{Z=3}^{\infty} \sum_{j=2}^{Z-1} \boldsymbol{R}_j \left(\frac{\partial F}{\partial \boldsymbol{R}_j} \right)_{T,\{N_i\},\{R_{i\neq j}\}} p(\{\boldsymbol{R}_i, N_i\}, Z; t)\, \mathrm{d}R_j\, \mathrm{d}N_j \quad (26)$$

where n is the number density of the polymer chains. The dangling end strands of the chain do not contribute to the stress.

The CUBS model used here has been shown[39] to be consistent with the two-generator, nonequilibrium thermodynamics formalism, general equation for the nonequilibrium reversible−irreversible coupling, GENERIC.[40−42] Hence, the model automatically satisfies many fundamental properties such as nonnegative entropy growth.

3. Brownian Dynamics Simulation

Analytic solution of the CUBS model is only possible in a small number of cases.[31] Therefore, a numerical algorithm is necessary in order to make predictions. Numerical solution of the Fokker−Planck (or, more accurately, differential Chapman−Kolmogorov) equation is, in general, not feasible. Note that the Fokker−Planck equation has $4Z-3$ independent variables for a chain with a given number of entanglements. A moderately entangled chain of $\langle Z \rangle = 20$ requires the numerical solution of the probability density in 77 dimensions! The real situation is much worse, however, because a chain with an average of 20 entanglements can easily fluctuate to have 40 entanglements, meaning that p in a 157-dimensional space must also be solved. On the other hand, we typically do not require full knowledge of the probability density, but rather only a few moments, such as that given in eq 26. Therefore, we derive a numerical Brownian dynamics algorithm to solve the equivalent stochastic differential equations.

As an initial condition for the Brownian dynamics simulation, we require an ensemble of chains whose statistics are described by the Maxwell−Boltzmann equation. It is possible to construct such an ensemble by using eqs 8−10. A detailed description of the chain initialization procedure can be found elsewhere.[30,36] In addition to this procedure, after creating the distribution of strand orientations ($\boldsymbol{Q}_i$), we reflect segments whose length is smaller than the length of a Kuhn. Our studies show that results are insensitive to this particular cutoff length, provided it is smaller than the average length of Q.

A comparison between simulated distributions and analytical expressions for Z and $\boldsymbol{Q}_i$ are given in the Supporting Information. We take these comparisons as verification of the code.

From eq 15, the evolution equation for the number of Kuhn steps in strand can be written as:

$$\mathrm{d}N_i = \frac{1}{k_\mathrm{B}T\tau_i}(\mu_{i+1} - \mu_i)\,\mathrm{d}t - \frac{1}{k_\mathrm{B}T\tau_{i-1}}(\mu_i - \mu_{i-1})\,\mathrm{d}t + \sqrt{\frac{2}{\tau_i}}\,\mathrm{d}W_i - \sqrt{\frac{2}{\tau_{i-1}}}\,\mathrm{d}W_{i-1} \qquad i = 1, ..., Z \quad (27)$$

where μ_i is the chemical potential of the ith strand, and τ_i is defined by eq 14. The chemical potential of the interior strand and the dangling end can be obtained from the free energy eqs 2 and 3, respectively.

$$\frac{\mu_\mathrm{S}(N_i, \boldsymbol{Q}_i)}{k_\mathrm{B}T} = -\frac{3\boldsymbol{Q}_i^{\,2}}{2N_i^{\,2}a_\mathrm{K}^{\,2}} + \frac{3}{2N_i} \quad (28)$$

$$\frac{\mu_\mathrm{E}(N_i)}{k_\mathrm{B}T} = -\frac{1}{2N_i} \quad (29)$$

By integrating eq 27 over a small time-step size Δt, we make an approximation for the first term on the right side,

$$N_i(t+\Delta t) \cong N_i(t) + \frac{\Delta t}{2k_\mathrm{B}T\tau_{i-1}}[\mu_{i-1}(t+\Delta t) - \mu_i(t+\Delta t) + \mu_{i-1}(t) - \mu_i(t)] + \frac{\Delta t}{2k_\mathrm{B}T\tau_i}[\mu_{i+1}(t+\Delta t) - \mu_i(t+\Delta t) + \mu_{i+1}(t) - \mu_i(t)] + \sqrt{\frac{2}{\tau_i(t)}}\Delta W_i(t) - \sqrt{\frac{2}{\tau_{i-1}(t)}}\Delta W_{i-1}(t) \qquad i = 1, ..., Z \quad (30)$$

where ΔW is the Wiener increment, which is a Gaussian-distributed random variable with zero mean and variance Δt.[35,43] Equation 30 represents Z-coupled, nonlinear (cubic), algebraic equations in the unknown $\{N_i(t+\Delta t)\}$, which cannot be solved analytically. We solve them numerically by using a multidimensional Newton−Raphson method.[44] To reduce the dimensionality of the problem, eq 30 can also be written as

$$N_i(t+\Delta t) = N_i(t) + \Delta n_{i-1} - \Delta n_i \quad (31)$$

where the Δn_i are defined as

$$\Delta n_i = \frac{-\Delta t}{2k_\mathrm{B}T\tau_i}[\mu_{i+1}(t+\Delta t) - \mu_i(t+\Delta t) + \mu_{i+1}(t) - \mu_i(t)] - \sqrt{\frac{2}{\tau_i(t)}}\Delta W_i(t) \quad (32)$$

The functions to be zeroed in the multidimensional Newton−Raphson method are expressed in dimensionless form as

$$F_i(t+\Delta t) = \Delta n_i + \frac{\Delta t}{(N_i(t) + N_{i+1}(t))}[\mu_{i+1}(t+\Delta t) - \mu_i(t+\Delta t)] + f_i(t) \quad (33)$$

where $f_i(t)$ is defined as:

$$f_i(t) = \frac{\Delta t}{(N_i(t) + N_{i+1}(t))}[\mu_{i+1}(t) - \mu_i(t)] + \frac{2\Delta W_i(t)}{\sqrt{N_i(t) + N_{i+1}(t)}} \quad (34)$$

Finally, the probabilities of creation and destruction of entanglements in a time step are given by

$$w^\mathrm{d} = 1 - \exp\left(-\frac{1}{\tau_\mathrm{e}} \sqrt{\frac{3N_\mathrm{e}}{N_\mathrm{E}}} \Delta t \right) \quad (35)$$

$$w^\mathrm{c} = 1 - \exp\left(-\frac{1}{\tau_\mathrm{e}} \sqrt{\frac{3}{N_\mathrm{e}N_\mathrm{E}}} (N_\mathrm{E} - 2)\Delta t \right) \quad (36)$$

where N_E is the number of Kuhn steps in a dangling end. The

algorithm is made dimensionless by using a characteristic length, $a_K\sqrt{N_e}$, a characteristic time, τ_e, and normalizing the number of Kuhn steps by N_e. Simulations are performed for an ensemble of identically prepared chains, and the averages are taken over the ensemble. The algorithm is order one-half in the time-step size for the Brownian dynamics of the Kuhn steps, first-order for the evolution of entanglement positions, and first-order for creation and destruction. The algorithm is stable and found to converge quickly for a time-step size of 0.02 τ_e. Time-step size convergence was also checked for a typical system. Equilibrium simulations were performed for times sufficient to relax all chains from their initial conformations, and statistics were checked (see the Supporting Information). Close agreement with analytic results were found.

The relaxation modulus, $G(t)$, is found directly from an equilibrium simulation by using a Green−Kubo expression from linear response theory[45]

$$G(t) = \frac{1}{nk_BT}\frac{1}{\lambda}\int_0^{\lambda} \langle \tau_{yx}(t_1)\tau_{yx}(t+t_1)\rangle_{eq}\, dt_1 \qquad (37)$$

where $\langle ...\rangle_{eq}$ indicates an average taken over a large ensemble of chains at equilibrium, and λ is the simulation time. The relaxation modulus thus obtained is fit to a relaxation spectrum

$$G(t) = \sum_i g_i \exp(-t/\lambda_i) \qquad (38)$$

where t is the time, g_i is a set of weighting factors, and λ_i are the corresponding time constants. We use either an implementation of the nonlinear least-squares (NLLS) Marquardt−Levenberg algorithm or a variation of CONTIN. Our results are insensitive to which method is used.

The set of $\{g_i, \lambda_i\}$ values obtained from this fit are then used for the prediction $G^*(\omega) = G'(\omega) + iG''(\omega)$, where $G'(\omega)$ and $G''(\omega)$ are the storage and loss moduli, respectively. Hence,

$$G'(\omega) = \sum_i \frac{g_i(\lambda_i\omega)^2}{1+(\lambda_i\omega)^2}, \qquad G''(\omega) = \sum_i \frac{g_i\lambda_i\omega}{1+(\lambda_i\omega)^2} \qquad (39)$$

Also, the relaxation spectrum can be used for generating a Cole−Cole plot, where the real part of the complex viscosity ($\eta^*(\omega) = \eta'(\omega) - i\eta''(\omega)$) is plotted against the imaginary part. $G'(\omega)$ and $G''(\omega)$ are related to $\eta'(\omega)$ and $\eta''(\omega)$ by,

$$G'(\omega) = \omega\eta''(\omega) \qquad G''(\omega) = \omega\eta'(\omega) \qquad (40)$$

Finally, for a homologous series of linear polymers, the relation between the zero-shear-rate viscosity and molecular weight is known to follow the form

$$\eta_0 = KM_w^{\ a} \qquad (41)$$

The exact value of the exponent a is still a matter of debate; reptation theory predicts a scaling of 3.0, while numerous experiments[46] suggest scaling between 3.3 and 3.6. However, many of the experiments used to estimate this exponent were performed on polydisperse systems, and the weight-averaged molecular weight was assumed in eq 41. Many numerical simulations[47,48] suggest a scaling of 3.4 ± 0.1. Tao et al.[49] reported an experimental value of 3.43 for concentrated hydrogenated polybutadiene blends. The primitive chain network model proposed by Masubuchi et al.[50] predicts a scaling of 3.5 ± 0.1, while the dual slip-link model of Doi and Takimoto[51] predicts a scaling of 3.45. Nonetheless, η_0 can be found from our spectrum, and the scaling prediction found for the CUBS model from the modulus

$$\eta_0 = \int_0^{\infty} G(t)\, dt \qquad (42)$$

The self-diffusion coefficient, D, of the center of mass of the polymer chain is defined as,[52]

$$D = \lim_{t\to\infty} \frac{1}{6t}\langle (\boldsymbol{R}_c(t) - \boldsymbol{R}_c(0))^2\rangle \qquad (43)$$

where $\boldsymbol{R}_c$ is the chain center of mass. Reptation theory predicts that the chain self-diffusion coefficient scales as,

$$D \sim \frac{\langle R^2\rangle}{\tau_d} \sim M_w^{\ -x} \qquad (44)$$

where $\langle R^2\rangle$ is the mean-square end-to-end length of the chain, and τ_d is the reptation time. The value of the exponent x predicted by pure reptation is 2. Experimental results suggest a stronger scaling of self-diffusion coefficient with M_w. Studies conducted on the diffusivity of concentrated hydrogenated polybutadiene reports the scaling of the exponent in the range −2.2 to −2.5, both in solution and in the melt.[49,53] The primitive chain network model[50] predicts a scaling of 2.4 ± 0.2.

Table 1. Properties of Polymer Systems

polymer system	M_w (g/mol)	PI[a]	temperature (°C)	$\langle Z\rangle_{eq}$	data collected by
PS1 melt	160 000	<1.05	160	9	Marin and Graessley, 1977[54]
PS2 melt	200 000	1.05	160	11	Nair, 2004[55]
PS3 melt	417 000	<1.10	160	23	Nair[b]
PS4 melt	670 000	<1.15	160	37	Marin and Graessley, 1977
PB1 melt	42 230	1.03	26	22	Juliani and Archer, 2001[56]
PB2 melt	43 850	1.01	40	32	Wang et al., 2003[57]
PB3 melt	60 900	1.05	26	32	Juliani and Archer, 2001
PIB melt	130 000	1.25	25	15	Venerus[b]
PS/TCP soln	1.92×10^6	1.20	23	10	Venerus and Kahvand, 1994[58]

[a] Polydispersity index. [b] Not published.

4. Experimental Systems

Comparisons are made with the experimental systems shown in Table 1. Simulations are performed with and without constraint release. For each system, the average number of chain segments at equilibrium is calculated as $\langle Z\rangle_{eq} = M_w/M_e$, where M_w is the weight-average molecular weight and M_e is molecular weight of the chain between two entanglements. For CUBS, we find that M_e can be estimated from the expression

$$M_e = \frac{4}{5}\frac{\rho RT}{G_N} \qquad (45)$$

where ρ is the polymer density, R is the gas constant, T is the temperature, and G_N is the plateau modulus, typically estimated as the value of the storage modulus at the frequency where the loss modulus is at a local minimum.

M_e^{melt} used for the polystyrene samples at 160 °C is ∼18 000 g/mol, and that for the polybutadiene sample at 26 °C is ∼1900 g/mol.[46] For the polybutadiene sample at 40 °C, $M_e^{melt} \sim 1375$ g/mol agreed more closely with the data. The polyisobutylene sample has $M_e^{melt} \sim 8900$ g/mol.[46] Also compared was a 12 wt % solution in tricresyl phosphate (TCP) of nearly monodisperse (polydispersity index = 1.2) polystyrene with a molecular weight M_w of 1.92×10^6 at a polymer density of 0.135 g/cm^3.

Table 2. Properties of Polymer Blends

polymer system	M_w (g/mol)	temperature (°C)	$\langle Z\rangle_{eq}$	data collected by
40/60 PS1	177 kDa, 60 kDa	170	10, 3	Maier et al. 1998[59]
50/50 PS2	670 kDa, 160 kDa	160	37, 9	Montfort et al., 1979[60]
50/50 PB	44 kDa, 12 kDa	40	32, 9	Wang et al., 2004[61]

Table 3. Properties of Polymer Melts

polymer melt	temperature (°C)	d_t (Å)	a_K (Å)	N_e
PS	140	76	16.2	22
PB	25	37	8.5	19
PIB	25	56	11.6	23

For solutions, we find that the entanglement molecular weight is well estimated by

$$M_e^{\text{solution}} \cong \frac{M_e^{\text{melt}}}{\phi^{1.3}} \tag{46}$$

where ϕ is the volume fraction of the polymer, and $M_e^{\text{melt}} \sim 18\,000$ g/mol.

The properties of the polymer blend systems are given in Table 2. Before simulation, the code requires estimates for the parameters N_K and N_e, as well as specification of the ensemble size, simulation time, and time-step size (Δt). The computational cost and statistical noise can be kept to a minimum by the proper selection of ensemble size and simulation time. The ensemble size is selected such that the total number of chain segments is approximately 50 000. For lower-molecular-weight polymers, the necessary simulation time is $\sim\langle Z\rangle_{eq}^3/\pi^2$ and for large molecular weights, it is approximately $2\langle Z\rangle_{eq}^3/\pi^2$. Simulations with constant entanglement friction are found to converge for a time-step size of $0.05\,\tau_e$, and those with constant chain friction are found to converge for $\Delta t = 0.02\,\tau_e$.

The parameter N_e for each polymer system is obtained from the relationship,[62]

$$N_e = \left(\frac{d_t}{a_K}\right)^2 \tag{47}$$

where d_t is the average end-to-end distance of the entanglement segment at equilibrium and a_K is the length of a Kuhn step. d_t is directly proportional[63] to the packing length p. The definition of d_t and p and their values at different temperatures for various polymer systems are tabulated in the literature.[63] The length of a Kuhn step, a_K, is obtained from the characteristic ratio through the relationship,[64]

$$C_\infty = \frac{a_K}{l} - 1 \tag{48}$$

where C_∞ is the characteristic ratio and l is the bond length. However, the calculations shown here do not require specification of the Kuhn step size. The calculated values of N_e for various polymer melts are tabulated in Table 3. In the case of PS solution, N_e is calculated as

$$N_e^{\text{solution}} = \frac{M_e^{\text{solution}}}{M_K} \tag{49}$$

where M_K is the molecular weight of a Kuhn step. By using the above expression, the value of N_e calculated for the PS solution at 25 °C is approximately 325. However, the simulation results are found to be independent of N_e for $N_e \geq 50$, and hence, N_e is taken as 50 to save computational cost.

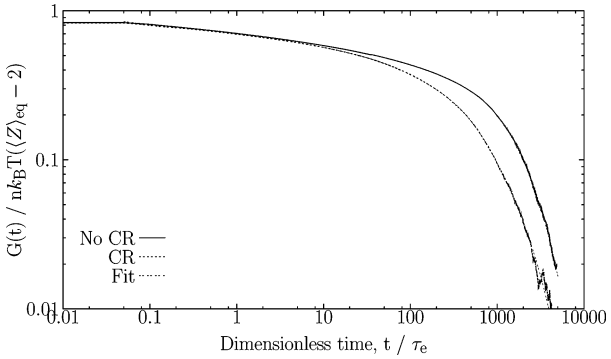

Figure 2. Relaxation modulus as a function of dimensionless time for $\langle Z\rangle_{eq} = 37$. Also shown are the fits to the simulation results with and without constraint release.

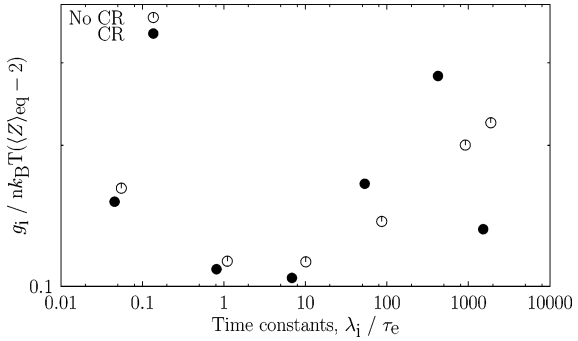

Figure 3. Discrete relaxation spectrum for the simulations with and without constraint release for $\langle Z\rangle_{eq} = 37$.

Chain conformations are generated assuming Gaussian strands. However, the number of Kuhn steps is generated assuming no cutoff in entanglement spacing size. To obtain a true equilibrium ensemble, it is necessary to equilibrate a few time steps before the real simulation begins. We equilibrate $\langle Z\rangle_{eq}\tau_e/\Delta t$ time steps, which is sufficient to create an equilibrium ensemble with cutoff in $\boldsymbol{Q}$.

5. Monodisperse Comparisons

The predictive power of the model is analyzed by comparing the $G^*(\omega)$ and the Cole−Cole predictions with experimental data. The single phenomenological parameter used in the model, τ_e, is estimated by fitting the $G^*(\omega)$ calculated from the simulation to the experimental data. All time scales in the simulation are normalized by τ_e, and all stresses by the relaxation modulus $nk_BT(\langle Z\rangle_{eq} - 2)$. Note that $nk_BT = \rho RT/M_w$, where ρ is the density of the polymer, and R, the gas constant. Adjusting τ_e does not affect the shapes of the storage and loss moduli, but rather determines only their horizontal locations on the log−log plot.

The relaxation moduli obtained from simulations with and without constraint release for $\langle Z\rangle_{eq} = 37$ are shown in Figure 2. It can be seen that inclusion of constraint release results in faster relaxation of the chains, by roughly a factor of 2, as suggested by double reptation expressions, and changes the shape slightly. Also shown in the figure are the fits of the relaxation moduli to eq 38. Figure 3 shows the corresponding relaxation spectra, where the dimensionless weights, $g_i/nk_BT(\langle Z\rangle_{eq} - 2)$, are plotted against the dimensionless time constants, λ_i/τ_e, and a qualitative difference can be seen in the spectra.

The storage and loss moduli predicted by the model are calculated from the relaxation spectrum by using eq 39. τ_e is estimated by fitting the model's $G'(\omega)$ curve to the experimental data. Figures 4 and 5 show the comparison of theoretical $G^*(\omega)$

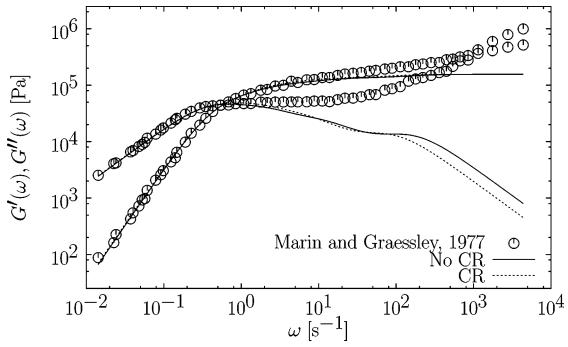

Figure 4. Comparison between $G^*(\omega)$ predictions of the model with and without constraint release and that for PS melt of $M_w = 160$ kDa and $\langle Z\rangle_{eq} = 9$ at 160 °C.

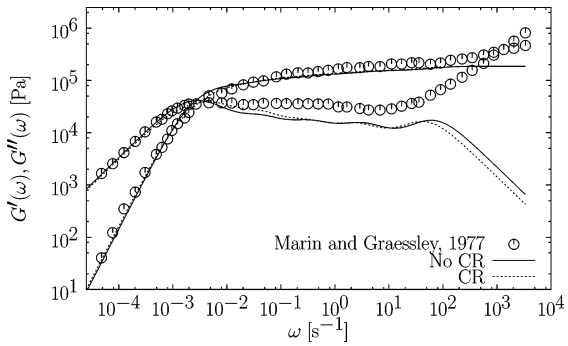

Figure 5. Comparison between $G^*(\omega)$ predictions of the model with and without constraint release and that for PS melt of $M_w = 670$ kDa and $\langle Z\rangle_{eq} = 37$ at 160 °C.

predictions with experimental data[54] for nearly monodisperse polystyrene melts of molecular weight 160 kDa and 670 kDa, respectively. The model shows good agreement with experimental data at lower frequencies, but fails to account for the glassy mode at high frequencies. The smallest time scale resolved by the model is that associated with the strand dynamics. The model is unable to capture relaxations more rapid than the Kuhn step shuffling. This coarse-graining contributes to the discrepancy from experiments at high frequencies in the plateau. Another contribution could be the fact that the model predictions are for purely monodisperse polymers, whereas the experimental data have some polydispersity.

To check the consistency of simulation results, $G(t)$ obtained from the simulation is compared with that calculated from the relaxation spectrum fit to the experimental data. The relaxation modulus for experimental data is calculated by using eq 38, where the set of $\{g_i, \lambda_i\}$ values are obtained by doing a fit to the $G^*(\omega)$ data. We do the fit to $G^*(\omega)$ data in two ways: by using a modified CONTIN algorithm and by using the rheological software IRIS. A fit to the data is shown in Figure 6, and Figure 7 gives a comparison between theory and experiments for PS melt of molecular weight 200 kDa and $\langle Z\rangle_{eq} = 11$ at 160 °C. Good agreement is found between the data and the simulation. There is a slight discrepancy between the two plots at short times, which is expected because of the coarse-graining imposed in the model.

Figures 8 and 9 show the G^* predictions and Cole−Cole plot, respectively, for nearly monodisperse polystyrene melts of molecular weight 200 kDa.[55] The model gives good agreement with experiments, again except at very high frequency. We can see that the effect of constraint release is more evident in the Cole−Cole plot. Figure 10 shows the Cole−Cole plot for nearly monodisperse polystyrene melts of molecular weight 417 kDa.

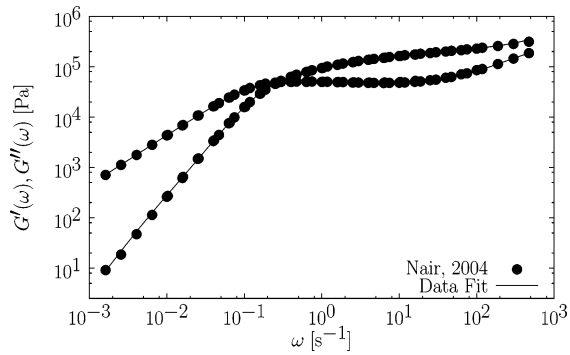

Figure 6. Fit to the $G^*(\omega)$ data of polystyrene melt of molecular weight 200 kDa and $\langle Z\rangle_{eq} = 11$ at 160 °C.

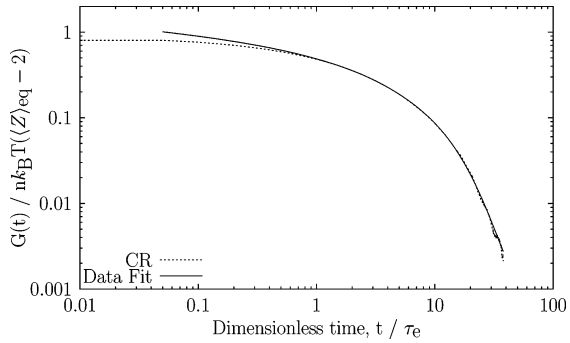

Figure 7. Comparison between the $G(t)$ predicted by the model with constraint release and that calculated for PS melt of M_w 200 kDa and $\langle Z\rangle_{eq} = 11$ at 160 °C.

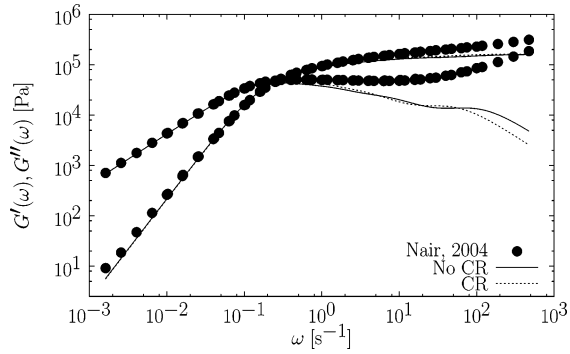

Figure 8. Comparison between $G^*(\omega)$ predictions of the model with and without constraint release and that for PS melt of $M_w = 200$ kDa and $\langle Z\rangle_{eq} = 11$ at 160 °C.

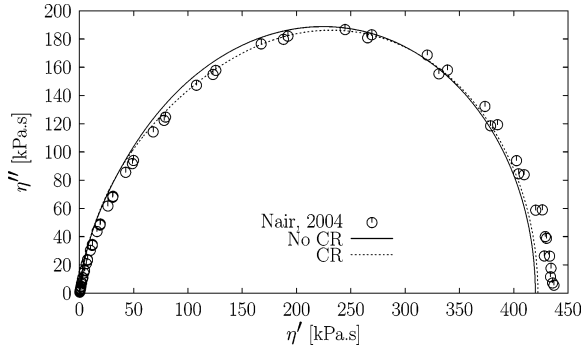

Figure 9. Cole−Cole plot of the model with and without constraint release and that of PS melt of molecular weight 200 kDa and $\langle Z\rangle_{eq} = 11$ at 160 °C.

Again, incorporation of constraint release improves slightly the model's ability to describe the data.

A comparison between the $G^*(\omega)$ predictions of the model and nearly monodisperse polybutadiene melts of M_n 41 kDa

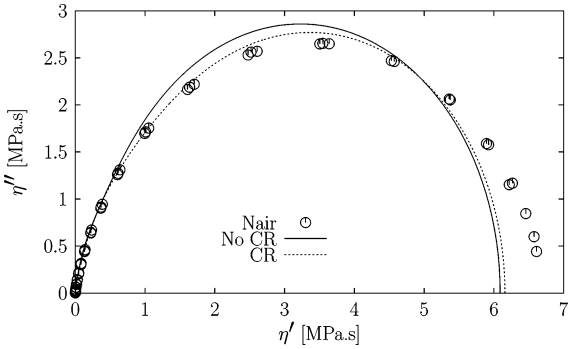

Figure 10. Cole−Cole plot of the model with and without constraint release and that of PS melt of molecular weight 417 kDa and $\langle Z\rangle_{eq}$ = 23 at 160 °C.

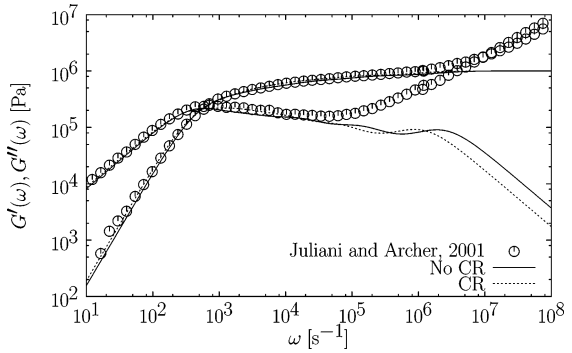

Figure 11. Comparison between $G^*(\omega)$ predictions of the model with and without constraint release and that for PB melt of M_n = 41 kDa and $\langle Z\rangle_{eq}$ = 22 at 26 °C.

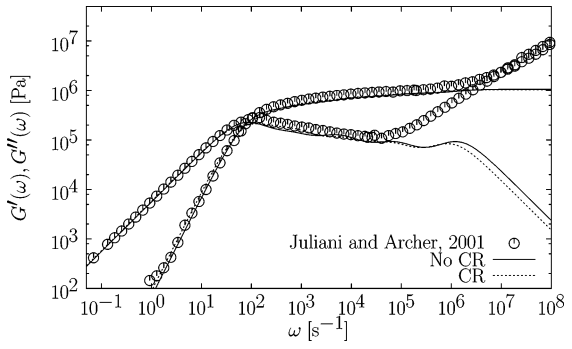

Figure 12. Comparison between $G^*(\omega)$ predictions of the model with and without constraint release and that for PB melt of M_n = 58 kDa and $\langle Z\rangle_{eq}$ = 32 at 26 °C.

and 58 kDa[56] are given in Figures 11 and 12, respectively. In both cases, the model shows excellent agreement with data over five decades in frequency. Figure 13 shows the Cole−Cole predictions for nearly monodisperse polybutadiene melts of molecular weight 44 kDa.[57] It is evident that inclusion of constraint release is necessary for quantitative agreement with highly entangled systems.

A comparison between theory and experiments for a polyisobutylene melt of molecular weight 130 kDa is given in Figure 14. The predictions of the model show a discrepancy in the storage modulus at low frequency. One reason for this discrepancy can be the slight amount of polydispersity in the experimental data or the unusual slope of the storage modulus at low frequency in the data.

Finally, in Figure 15, comparisons of the $G^*(\omega)$ predictions of the model and that of a lightly entangled polystyrene solution[58] are shown.

We also calculated the zero-shear-rate viscosity, η_0, as a function of molecular weight as predicted by our model and

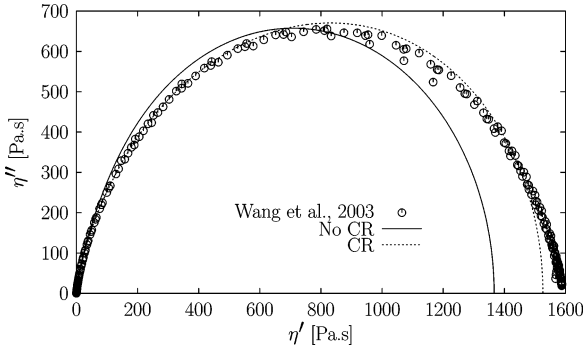

Figure 13. Cole−Cole plot of the model with and without constraint release and that of PB melt of molecular weight 44 kDa and $\langle Z\rangle_{eq}$ = 32 at 40 °C.

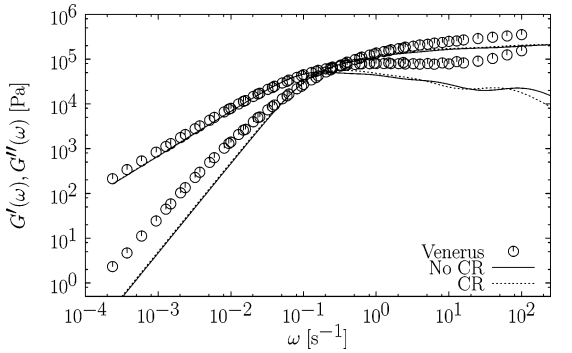

Figure 14. Comparison between $G^*(\omega)$ predictions of the model with and without constraint release and that for PIB melt of M_w = 130 kDa and $\langle Z\rangle_{eq}$ = 15 at 25 °C.

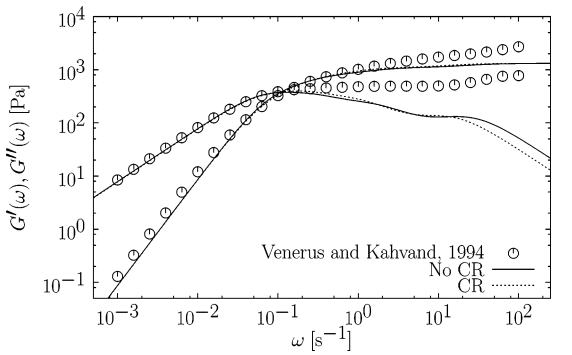

Figure 15. Comparison between $G^*(\omega)$ predictions of the model with and without CR and that for 12 wt % PS/TCP solution of M_w = 1.92 × 10^6, $\langle Z\rangle_{eq}$ = 10 at 23 °C.

compared it with experimental data for linear polystyrene melts. The zero-shear-rate viscosity is calculated as

$$\eta_0 = \sum_i g_i \lambda_i \tag{50}$$

Figure 16 shows good agreement with the observed scaling of the zero-shear-rate viscosity with molecular weight. In this plot, τ_e is estimated by averaging the values to the fits of the $G^*(\omega)$ data above. Predictions are made at a temperature of 160 °C. Both the predicted and experimental values of the exponent are found to be greater than 3.4: $\eta_0 \propto M_w^{3.67}$.

In Figure 17, the dimensionless self-diffusion coefficients predicted by the model with and without constraint release are given. Because the time scales and length scales in our simulation are made dimensionless by τ_e and $N_e a_K^2$, respectively, we plot $D\tau_e/N_e a_K^2$ as a function of $\langle Z\rangle_{eq}$. Neglecting $\langle Z\rangle_{eq}$ below 15, our model predicts an exponent of −2.5, while inclusion of

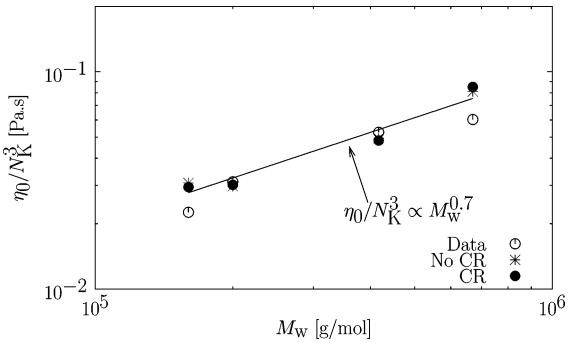

Figure 16. Comparison between the zero-shear viscosity scaling of experiments and that predicted by the model for linear polystyrene melts at 160 °C. Data from Marin and Graessley, 1977,[54] and Nair, 2004.[55]

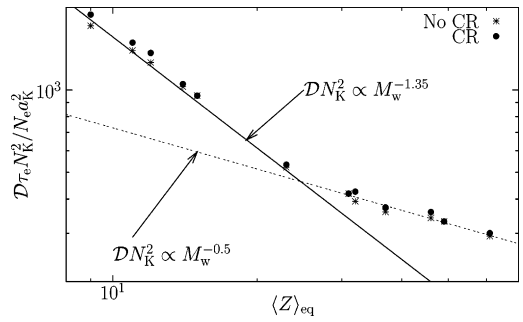

Figure 17. Self-diffusion constant scaling predicted by the model with and without constraint release for linear polystyrene melts at 160 °C.

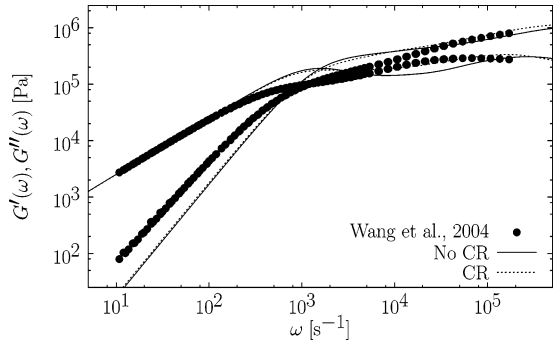

Figure 18. Comparison between $G^*(\omega)$ predictions of the model with and without CR and that for PB blend of M_w 44 kDa/12 kDa, 50 wt %, and $\langle Z \rangle_{eq} = 32/9$ at 40 °C.

lower $\langle Z \rangle_{eq}$ gives a stronger exponent of -3. Incorporation of constraint release does not affect the scaling.

We note in passing that incorporation of constant chain friction into the model does not have much effect on the linear viscoelastic predictions (shown in Supporting Information). However, nonlinear predictions of the model (not shown in this paper) are improved very slightly with the introduction of constant chain friction, which is typically assumed in tube models.

6. Bidisperse Comparisons

Having shown the ability of the CUBS model to explain experimental trends in the linear viscoelasticity of monodisperse polymers, we now check predictions for binary blends. Figures 18 and 19 show the G^* predictions and Cole−Cole plot, respectively, for a bimodal blend of polybutadiene[61] of M_w 44 kDa/12 kDa, 50 wt % of each fraction. Figure 20 shows a comparison of the $G^*(\omega)$ predictions for a polystyrene blend of M_w 177 kDa/60 kDa, 40 wt % of the high-molecular-weight fraction,[59] and Figure 21 shows that for another polystyrene

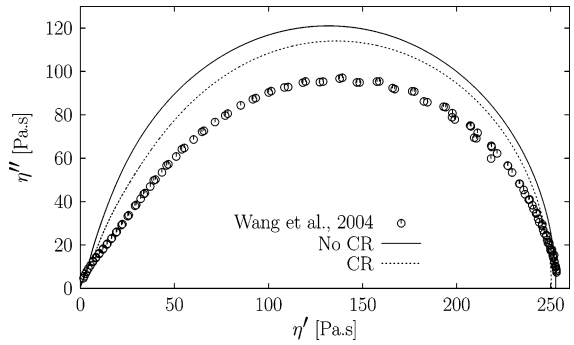

Figure 19. Cole−Cole plot of the model with and without constraint release and that of a bimodal PB blend of M_w 44 kDa/12 kDa, 50 wt %, and $\langle Z \rangle_{eq} = 32/9$ at 40 °C.

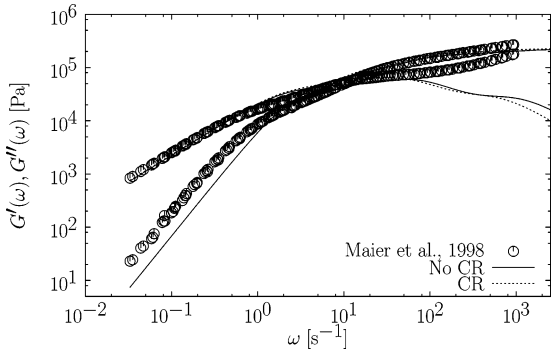

Figure 20. Comparison between $G^*(\omega)$ predictions of the model with and without CR and that for PS blend of M_w 177 kDa/60 kDa, 40/60 wt %, and $\langle Z \rangle_{eq} = 10/3$ at 170 °C.

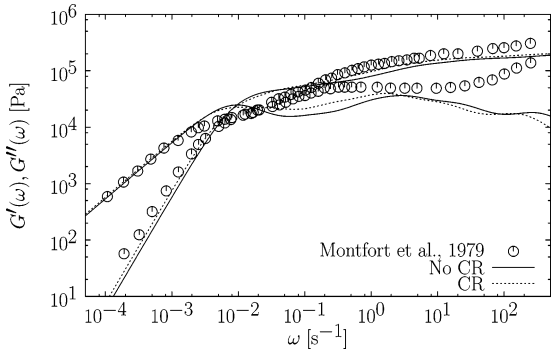

Figure 21. Comparison between $G^*(\omega)$ predictions of the model with and without CR and that for PS blend of M_w 670 kDa/160 kDa, 50 wt %, and $\langle Z \rangle_{eq} = 37/9$ at 160 °C.

blend of M_w 670 kDa/160 kDa, 50 wt % of each fraction.[60] We see that the theory predicts the shift in the relaxation time of the higher-molecular-weight component qualitatively. However, the overall prediction suggests that there are still some features missing in the model for the blend.

The discrepancy prompted us to do a comparison of the relaxation modulus. In Figure 22, the relaxation moduli for simulations with and without constraint release are given for the polybutadiene blend of M_w 44 kDa/12 kDa. The hump seen in these plots is a clear indication of two characteristic relaxations, each corresponding to the relaxation of individual species present in the mixture. These two modes are also visible in the spectrum shown in the Supporting Information. A fit to the $G^*(\omega)$ data for this blend shown in the Supporting Information and the set of $\{g_i, \lambda_i\}$ values obtained from the fit are used for calculating the relaxation modulus predicted by the experimental data. A comparison between the relaxation modulus predicted by the model with constraint release, and

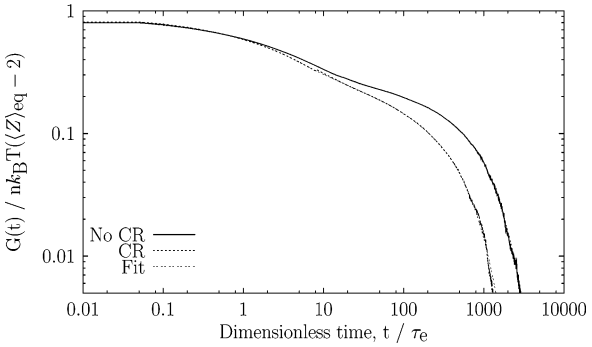

Figure 22. Dimensionless relaxation modulus vs dimensionless time for PB blend of M_w 44 kDa/12 kDa, 50 wt %, and $\langle Z\rangle_{eq} = 32/9$ at 40 °C. Also shown are the fits to the simulations with and without CR.

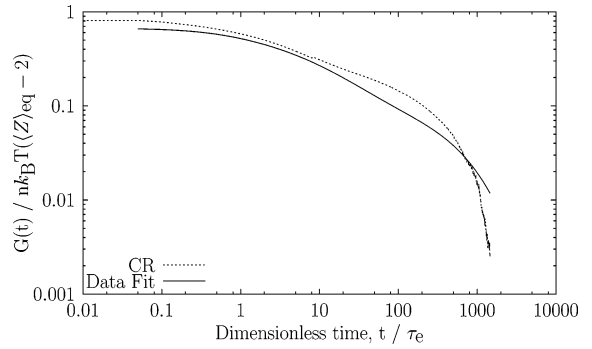

Figure 23. Comparison between the relaxation modulus predicted by the model with constraint release and that calculated for bidisperse polybutadiene blend of molecular weight 44 kDa/12 kDa, 50 wt %, and $\langle Z\rangle_{eq} = 32/9$ at 40 °C.

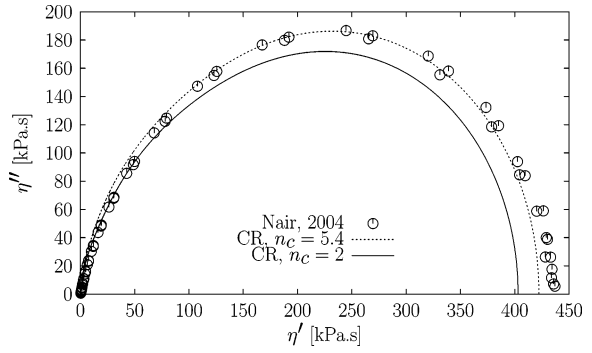

Figure 24. Cole−Cole plot of the model with $n_c = 5.4$ and $n_c = 2$ and that of PS melt of molecular weight 200 kDa and $\langle Z\rangle_{eq} = 11$ at 160 °C.

that calculated for the data is given in Figure 23. As evident from the figure, the theory underpredicts the relaxation time and overpredicts the plateau modulus, which in turn accounts for the discrepancy in the $G^*(\omega)$ predictions.

Recall that previous studies incorporating Rouse-like motions for the tube to mimic constraint release assumed that entanglements are binary interactions, whereas we assumed that 5.4 chains make up an entanglement. To examine these two assumptions more carefully, we also performed some calculations by assuming binary interactions in our slip-link model. Figure 24 compares these two assumptions for a moderately entangled polystyrene melt. Here, we see that the Cornet criterion is clearly superior to the binary assumption. On the other hand, a more entangled binary-blend PS melt shows somewhat closer agreement with $n_c = 2$ predictions, Figure 25. A definitive conclusion would probably require either a more narrow distribution of molecular weights, or an accurate accounting of the mild polydispersity seen in these samples.

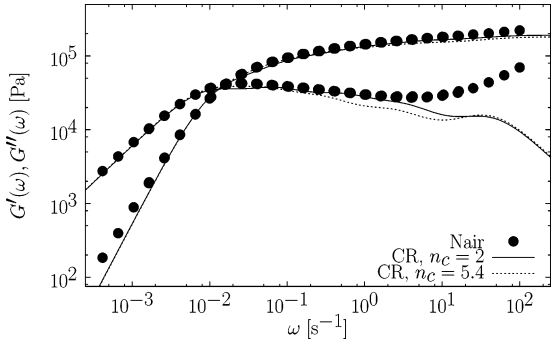

Figure 25. Comparison between $G^*(\omega)$ predictions of the model with $n_c = 5.4$ and $n_c = 2$ and that for PS melt of $M_w = 417$ kDa and $\langle Z\rangle_{eq} = 23$ at 160 °C.

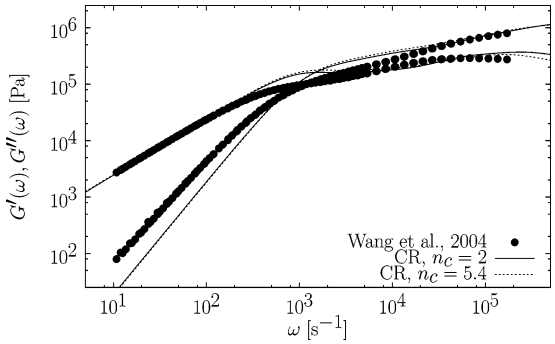

Figure 26. Comparison between $G^*(\omega)$ predictions of the model with $n_c = 5.4$ and $n_c = 2$ and that for PB blend of M_w 44 kDa/12 kDa, 50 wt %, and $\langle Z\rangle_{eq} = 32/9$ at 40 °C.

However, we do see that the predictions are not strongly sensitive to this assumption. The same conclusion can be drawn from the bidisperse comparison shown in Figure 26.

7. Conclusions

We introduce a consistently unconstrained Brownian slip-link model (CUBS) with constant chain friction and constraint release to study the viscoelastic properties of linear entangled monodisperse and bidisperse polymer liquids. As a full-chain model, it incorporates naturally segment connectivity, chain-length fluctuations, and chain stretching without additional parameters. Instead, the model requires a single phenomenological parameter, the characteristic time τ_e. A mean-field implementation of constraint release is considered. Although the model may also be used to predict flows, we restrict ourselves here to study only linear viscoelasticity.

The introduction of constant *chain* friction, as opposed to constant *entanglement* friction, does not significantly affect the linear viscoelastic predictions, whereas constraint release improves the results. Also, the qualitative effect of constraint release increases with increasing molecular weight.

The studies conducted on monodisperse polystyrene and polybutadiene melts and polystyrene solutions show good agreement with experimental data at all frequencies except the glassy modes. The discrepancy seen at higher frequencies can be attributed to the coarse-grained level of description incorporated in the model. In other words, at high frequencies, the characterization of a free energy by just the number of Kuhn steps and connector vector becomes questionable. The model predictions for polyisobutylene are encouraging; however, there is some discrepancy in the storage modulus predictions at low frequency. Likhtman and McLeish attributed discrepancies with their predictions and PIB data to a possible nonuniversality. However, we suspect that the discrepancies seen here might

also be attributable to polydispersity and possible uncertainty in the loss modulus at low frequencies.

The model is successful in explaining the experimental trends in polystyrene and polybutadiene blends qualitatively, but quantitative comparisons show limitations in the theory. A comparison of the relaxation modulus shows that the model underpredicts the decrease in relaxation times of long chains from the presence of short chains. Also, the plateau modulus exhibits an effective decrease not shown by the model. This leads us to suspect that some additional physics might be missing in the standard tube picture. Before adding new physics, however, we are currently exploring the consequences of other assumptions made in the theory. In particular, it is not necessary to mimic the CR process by diffusion. Also, assumptions about the creation and destruction at the ends of the chain can be removed.

Finally, the predicted diffusivity and viscosity scaling with molecular weight included a mild surprise. Namely, we find that the model predicts a viscosity scaling exponent of 3.6−3.7 for PS melts, somewhat higher than the commonly cited vale of 3.4. What is surprising is that the monodisperse samples studied here agree with this higher value. Also, the diffusion scaling relation $D \propto M_w^{-2.5}$ is in agreement with observation. Both of these results are not affected significantly by constraint release.

Acknowledgment. This material is based upon work supported by the National Science Foundation under grant no. NSF−OCI 0506305. We would like to acknowledge useful discussions with Professors Masao Doi and David Venerus.

Supporting Information Available: Calculation of constraint release prefactor, calculation of number of chain interactions in an entanglement, and supporting figures. This material is available free of charge via the Internet at http://pubs.acs.org.

References and Notes

(1) de Gennes, P. G. *J. Chem. Phys.* **1971**, *55*, 572−579.
(2) Edwards, S. F. *Proc. Phys. Soc., London* **1967**, *92*, 9−16.
(3) Doi, M.; Edwards, S. F. *J. Chem. Soc., Faraday Trans. 2* **1978**, *74*, 1789−1801.
(4) Doi, M.; Edwards, S. F. *J. Chem. Soc., Faraday Trans. 2* **1978**, *74*, 1802−1817.
(5) Doi, M.; Edwards, S. F. *J. Chem. Soc., Faraday Trans. 2* **1978**, *74*, 1818−1832.
(6) Doi, M.; Edwards, S. F. *J. Chem. Soc., Faraday Trans. 2* **1979**, *75*, 38−54.
(7) Marrucci, G. *J. Polym. Sci., Polym. Phys. Ed.* **1985**, *23*, 59−177.
(8) Tsenoglou, C. *Am. Chem. Soc. Polym. Prepr.* **1987**, *28*, 185−186.
(9) des Cloizeaux, J. *J. Europhys. Lett.* **1988**, *5*, 437−442.
(10) Rubinstein, M.; Colby, R. H. *J. Chem. Phys.* **1988**, *89*, 5291−5306.
(11) Marrucci, G.; Grizzuti, N. *Gazz. Chim. Ital.* **1988**, *118*, 179−185.
(12) Öttinger, H. C. *Phys. Rev. E* **1994**, *50*, 4891−4895.
(13) Mead, D. W. *J. Rheol.* **1996**, *40*, 633−663.
(14) Marrucci, G. *J. Non-Newtonian Fluid Mech.* **1996**, *62*, 279−289.
(15) Ianniruberto, G.; Marrucci, G. *J. Non-Newtonian Fluid Mech.* **1996**, *65*, 241−246.
(16) Hua, C. C.; Schieber, J. D. *J. Chem. Phys.* **1998**, *109*, 10018−10027.
(17) Hua, C. C.; Schieber, J. D.; Venerus D. C. *J. Chem. Phys.* **1998**, *109*, 10028−10032.
(18) Milner, S. T.; McLeish, T. C. B. *Phys. Rev. Lett.* **1998**, *81*, 725−728.
(19) Mead, D. W.; Larson, R. G.; Doi, M. *Macromolecules* **1998**, *31*, 7895−7914.
(20) Hua, C. C.; Schieber, J. D.; Venerus D. C. *J. Rheol.* **1999**, *43*, 701−717.
(21) Neergaard, J.; Park, K.; Venerus, D. C.; Schieber, J. D. *J. Rheol.* **2000**, *44*, 1043−1053.
(22) Ianniruberto, G.; Marrucci, G. *J. Non-Newtonian Fluid Mech.* **2000**, *95*, 363−374.
(23) Ianniruberto, G.; Marrucci, G. *J. Rheol.* **2001**, *45*, 1305−1318.
(24) Likhtman, A. E.; McLeish, T. C. B. *Macromolecules* **2002**, *35*, 6332−6343.
(25) Graessley, W. W. *Adv. Polym. Sci.* **1982**, *47*, 67−117.
(26) Orwoll, R. A.; Stockmayer, W. H. *Adv. Chem. Phys.* **1969**, *15*, 305−324.
(27) Bird, R. B.; Curtiss, C. F.; Armstrong, R. C.; Hassager, O. *Dynamics of Polymeric Liquids, Vol. 2: Kinetic Theory*; Wiley-Interscience: New York, 1987.
(28) Heuzey, M.-C.; Wood-Adams, P.; Sekki, D. *J. Appl. Sci.* **2004**, *94*, 569−586.
(29) Neergaard, J.; Schieber, J. D. In *Proceedings of the 13th International Congress on Rheology*; Binding, D. M., Hudson, N. E., Mewis, J., Piau, J. M., Petrie, C. J. S., Townsend, P., Wagner, M., Eds.; British Society of Rheology: Glasgow, UK, 2000.
(30) Schieber, J. D.; Neergaard, J.; Gupta, S. *J. Rheol.* **2003**, *47*, 213−233.
(31) Schieber, J. D. *J. Chem. Phys.* **2003**, *118*, 5162−5166. Our eq 9 comes from this paper and is the probability that a chain is selected at random and that one of the strands has *N* Kuhn steps. A different expression can be found for the probability of a strand chosen at random having *N* Kuhn steps.
(32) Vrahopoulou, E. P.; McHugh, A. J. *J. Rheol.* **1987**, *31*, 371−384.
(33) Green, M. S.; Tobolsky, A. V. *J. Chem. Phys.* **1946**, *14*, 80−92.
(34) Schieber, J. D.; Nair, D. In *Proceedings of the 14th International Congress on Rheology*, Aug 22−27, 2004; Korean Society of Rheology: Seoul, Korea, 2004.
(35) Gardiner, C. W. *Handbook of Stochastic Methods for Physics, Chemistry and the Natural Science*, 2nd ed.; Springer-Verlag: Berlin, Heidelberg, 1985.
(36) Gupta, S. Brownian Dynamics Simulation of a Full-Chain Temporary Network Model with Fixed Slip-links. M.S. Thesis, Illinois Institute of Technology, Chicago, 2002.
(37) Fetters, L. J.; Lohse, D. J.; Milner, S. T.; Graessley, W. W. *Macromolecules* **1999**, *32*, 6847−6851.
(38) Rault, J. *J. Non-Newtonian Fluid Mech.* **1987**, *23*, 229−247.
(39) Schieber, J. D. *J. Non-Equilib. Thermodyn.* **2003**, *28*, 1−10.
(40) Kaufman, A. N. *Phys. Lett. A* **1984**, *100*, 419−422.
(41) Grmela, M.; Öttinger, H. C. *Phys. Rev. E* **1997**, *56*, 6620−6632.
(42) Öttinger, H. C.; Grmela, M. *Phys. Rev. E* **1997**, *56*, 6633−6555.
(43) Öttinger, H. C. *Stochastic Processes in Polymeric Fluids*; Springer: Berlin, 1996.
(44) Press, W. H.; Teukolsky, S. A.; Vetterling, W. T.; Flannery, B. P. *Numerical Recipes in FORTRAN: The Art of Scientific Computing*, 2nd ed.; Cambridge University Press: New York, 1992.
(45) Résibois, P.; De Leener, M. *Classical Kinetic Theory of Fluids*; Wiley-Interscience: New York, 1977.
(46) Ferry, J. D. *Viscoelastic Properties of Polymers*, 3rd ed.; John Wiley & Sons: New York, 1980.
(47) Rubinstein, M. *Phys. Rev. Lett.* **1987**, *59*, 1946−1949.
(48) Deutsch, J. M.; Madden, T. L. *J. Chem. Phys.* **1989**, *91*, 3252−3257.
(49) Tao, H.; Lodge, T. P.; von Meerwall, E. D. *Macromolecules* **2000**, *33*, 1747−1758.
(50) Masubuchi, Y.; Takimoto, J.; Koyama, K.; Ianniruberto, G.; Marrucci, G.; Greco, F. *J. Chem. Phys.* **2001**, *115*, 4387−4394.
(51) Doi, M.; Takimoto, J.-I. *Philos. Trans. R. Soc. London, Ser. A* **2003**, *361*, 641−652.
(52) Doi, M.; Edwards, S. F. *The Theory of Polymer Dynamics*; Clarendon Press: Oxford, 1986.
(53) Lodge, T. P. *Phys. Rev. Lett.* **1999**, *83*, 3218−3221.
(54) Marin, G.; Graessley, W. W. *Rheol. Acta* **1977**, *16*, 527−533.
(55) Nair, R. R. Step Strain Rheology of Entangled Polymer Liquids. M.S. Thesis. Illinois Institute of Technology: Chicago, 2004.
(56) Juliani, J.; Archer, L. A. *J. Rheol.* **2001**, *45*, 691−708.
(57) Wang, S.; Wang, S.-Q.; Halasa, A.; Hsu, W.-L. *Macromolecules* **2003**, *36*, 5355−5371.
(58) Venerus, D. C.; Kahvand, H. *J. Polym. Sci., Polym. Phys. Ed.* **1994**, *32*, 1531−1542.
(59) Maier, D.; Eckstein, A.; Friedrich, Cr.; Honerkamp, J. *J. Rheol.* **1998**, *42*, 1153−1173.
(60) Montfort, J. P.; Marin, G.; Arman, J.; Monge, Ph. *Rheol. Acta* **1979**, *18*, 623−628.
(61) Wang, S.; von Meerwall, E. D.; Wang, S.-Q.; Halasa, A.; Hsu, W.-L.; Zhou, J. P.; Quirk, R. P. *Macromolecules* **2004**, *37*, 1641−1651.
(62) Fang, J.; Kroger, M.; Öttinger, H. C. *J. Rheol.* **2000**, *44*, 1293−1317.
(63) Fetters, L. J.; Lohse, D. J.; Colby, R. H. *Physical Properties of Polymers Handbook*; Mark, J. E., Ed.; AIP: New York, 1996.
(64) Flory, P. J. *Statistical Mechanics of Chain Molecules*; Hanser Publishers: Munich, 1988.

MA0519056

CDV